Available online at www.sciencedirect.com
ScienceDirect
Journal of Power Sources 180 (2008) 909–916
JOURNAL OF POWER SOURCES
www.elsevier.com/locate/jpowsour

Effect of electrode configuration on the thermal behavior of a lithium-polymer battery☆

Ui Seong Kim[a], Chee Burm Shin[a,*], Chi-Su Kim[b]

[a] *Department of Chemical Engineering and Division of Energy Systems Research, Ajou University, Suwon 443-749, Republic of Korea*
[b] *VK Corporation, Battery R&D Center, Pyeongtaek 450-090, Republic of Korea*

Received 15 July 2007; received in revised form 6 September 2007; accepted 16 September 2007
Available online 22 September 2007

Abstract

A thermal modeling was performed to study the effect of the electrode configuration on the thermal behavior of a lithium-polymer battery. It was examined the effect of the configuration of the electrodes such as the aspect ratio of the electrodes and the placing of current collecting tabs as well as the discharge rates on the thermal behavior of the battery. The potential and current density distribution on the electrodes of a lithium-polymer battery were predicted as a function of discharge time by using the finite element method. Then, based on the results of the modeling of potential and current density distributions, the temperature distributions of the lithium-polymer battery were calculated. The temperature distributions from the modeling were in good agreement with those from the experimental measurement for the batteries with three different types of electrodes at the discharge rates of 1*C*, 3*C*, and 5*C*.

Keywords: Lithium-polymer battery; Thermal behavior; Model; Electrode configuration; Finite element method

1. Introduction

The lithium-polymer battery is a preferred candidate as a power source for hybrid electric vehicle (HEV) and electric vehicle (EV) due to its outstanding characteristics such as high energy density, high voltage, low self-discharge rate, and good stability among others. However, much larger lithium-polymer batteries than those available in the market for consumer electronics are required for HEV and EV applications. Because the primary challenge in designing larger lithium-polymer batteries is safety, thermal stability problems must be overcome. The main concern with the thermal behavior of lithium-polymer battery is the possible significant temperature increase during high power extraction, which may cause battery degradation and thermal runaway. Thermal modeling can play a vital role to maintain the operating temperature and temperature uniformity of lithium-polymer battery within a suitable range [1–3].

There have been many previous efforts on the thermal modeling of lithium-polymer batteries for HEV and EV applications [4–14]. A one-dimensional thermal model assumes that temperature gradient is negligible in the two directions parallel to the current collectors [4–7]. Such an assumption may be valid for small-scale batteries. However, that assumption may not be justified for large-scale batteries, since the temperature distribution becomes more non-uniform as the electrode size of a battery increases. Then, a two- or three-dimensional thermal model may be desirable for large-scale batteries [8–14].

In this work, a two-dimensional modeling is performed to calculate the potential and current density distribution on the electrodes of a lithium-polymer battery comprising a $Li[NiCoMn]O_2$ positive electrode, a graphite negative electrode, and a plasticized electrolyte by following the same procedure of Kwon et al. [15]. They adopted a relatively simpler modeling approach by considering only Ohm's law and charge conservation on the electrodes based on the simplified polarization characteristics of the electrodes as compared to the previously published papers by other researchers [16–24]. The modeling of the potential and current density distributions on the elec-

☆ Selected Papers Presented at the 3rd INTERNATIONAL CONFERENCE ON POLYMER BATTERIES-FUEL CELLS (PBFC 2007).

* Corresponding author. Tel.: +82 31 219 2388; fax: +82 31 219 1612.
E-mail address: cbshin@ajou.ac.kr (C.B. Shin).

0378-7753/$ – see front matter © 2007 Elsevier B.V. All rights reserved.
doi:10.1016/j.jpowsour.2007.09.054

trodes is validated by the comparison between experimental and modeling discharge curves at the discharge rates of 1C, 3C, and 5C. Then, the thermal modeling of the lithium-polymer battery is carried out, which accounts for the ohmic heating due to the current flow on the electrodes and the heat generated due to the charge transfer at the electrode/electrolyte interface. The heat generation rate is calculated using the results of the modeling of potential and current density distributions.

2. Mathematical model

Fig. 1 shows a photograph of the 10 Ah lithium-polymer battery from VK Corporation that is modeled. Because the battery consists of the same repeating units of positive and negative electrode plates, polymer electrolytes and separators, we have chosen to model a cell composed of two parallel plate electrodes of the battery shown in Fig. 2. In Figs. 1 and 2, the current collecting tabs are the current collectors extending outside from the rectangular electrodes and they do not contain the electrode (active) material. A schematic diagram of the current flow in the cell during discharge is illustrated in Fig. 2. The distance between the electrodes is assumed to be so small that the current flow between the electrodes is perpendicular to the electrodes. The modeling procedure to calculate the potential and current density distribution on the electrodes is the same used by Kwon et al. [15]. From the continuity of current on the electrodes, the

Fig. 1. Photograph of the 10 Ah lithium-polymer battery from VK Corporation.

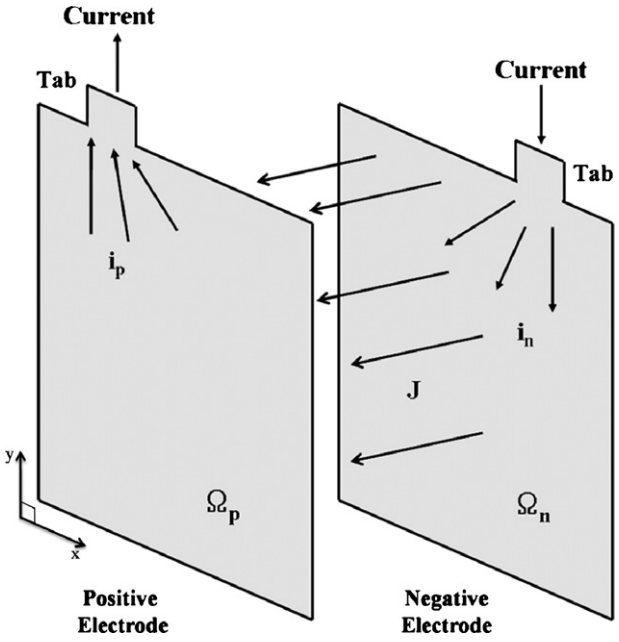

Fig. 2. Schematic diagram of the current flow in the parallel plate electrodes of a battery.

following equations can be derived

$$\nabla \vec{i}_p - J = 0 \quad \text{in } \Omega_p \tag{1}$$

$$\nabla \vec{i}_n + J = 0 \quad \text{in } \Omega_n \tag{2}$$

where $\vec{i}_p$ and $\vec{i}_n$ are the linear current density vectors (current per unit length ($A\,m^{-1}$)) in the positive and negative electrodes, respectively, and J is the current density (current per unit area ($A\,m^{-2}$)) transferred through the separator from the negative electrode to the positive electrode. Ω_p and Ω_n denote the domains of the positive and negative electrodes, respectively. By Ohm's law, $\vec{i}_p$ and $\vec{i}_n$ can be written as

$$\vec{i}_p = -\frac{1}{r_p}\nabla V_p \quad \text{in } \Omega_p \tag{3}$$

$$\vec{i}_n = -\frac{1}{r_n}\nabla V_n \quad \text{in } \Omega_n \tag{4}$$

where r_p and r_n are the resistances (Ω) of the positive and negative electrodes, respectively, and V_p and V_n are the potentials (V) of the positive and negative electrodes, respectively. By substituting Eqs. (3) and (4) into Eqs. (1) and (2), the following Poisson equations for V_p and V_n are obtained

$$\nabla^2 V_p = -r_p J \quad \text{in } \Omega_p \tag{5}$$

$$\nabla^2 V_n = +r_n J \quad \text{in } \Omega_n \tag{6}$$

The relevant boundary conditions for V_p and V_n are given in Ref. [15].

The resistance, r (r_p or r_n), are calculated as follows

$$r = \frac{1}{h_c S_c + h_e S_e} \tag{7}$$

Table 1
Parameters used for the calculation of electrode resistances

Parameter	Li_xC_6	$Li[NiMnCo]O_2$
S_e (S cm^{-1})	1.0	0.139
h_e (μ)	145	150
S_c (S cm^{-1})	6.33×10^5	3.83×10^5
h_c (μ)	10	20

where h_c and h_e are the thicknesses (m) of the current collector and the electrode material, respectively, and S_c and S_e are the electrical conductivities (S m^{-1}) of the current collector and the electrode material, respectively. The parameters used in the calculations of resistances for the electrodes are listed in Table 1 [15,23,24].

The current density, J, of Eqs. (5) and (6) is the function of the potential difference between the positive and negative electrodes ($V_p - V_n$). The functional form depends on the polarization characteristics of the electrodes. In this study, the following polarization expression used by Tiedemann and Newman [25] and Newman and Tiedemann [18] was adopted

$$J = Y(V_p - V_n - U) \tag{8}$$

where Y and U are the fitting parameters. As suggested by Gu [26], U and Y were expressed as the following functions of the depth of discharge (DOD)

$$U = a_0 + a_1(\mathrm{DOD}) + a_2(\mathrm{DOD})^2 + a_3(\mathrm{DOD})^3 \tag{9}$$

$$Y = a_4 + a_5(\mathrm{DOD}) + a_6(\mathrm{DOD})^2 \tag{10}$$

where $a_0 \sim a_6$ are the constants to be determined by experiments.

By solving the equations listed previously, the distribution of the current density, J, on the electrodes can be obtained as a function of the position on the electrode and the time. Therefore, DOD varies along with the position on the electrode and the time elapsed during discharge. The distribution of DOD on the electrode can be calculated from the distribution of J as

$$\mathrm{DOD} = \frac{\int_0^t J\,\mathrm{d}t}{Q_T} \tag{11}$$

where t is the discharge time (s) and Q_T is the theoretical capacity per unit area (Ah m^{-2}) of the electrodes.

Based on the differential energy conservation for a battery, the transient two-dimensional equation of heat conduction can be written as follows:

$$\rho C_p \frac{\partial T}{\partial t} = \frac{\partial}{\partial x}\left(k_x \frac{\partial T}{\partial x}\right) + \frac{\partial}{\partial x}\left(k_x \frac{\partial T}{\partial x}\right) + q - q_{conv} \tag{12}$$

where ρ is the density (kg m^{-3}), C_p the volume averaged specific heat capacity at constant pressure (J kg^{-1} °C^{-1}), T the temperature (°C), k_x and k_y is the effective thermal conductivities along the x and y directions (refer Fig. 2 for the x and y directions) (W m^{-1} °C^{-1}), respectively, q the heat generation rate per unit volume (W m^{-3}) and q_{conv} is the heat dissipation rate (W m^{-3}) through the surfaces of the battery by convection. Effective thermal conductivities of various compartment of the cell can be estimated based on the equivalent networks of parallel and series thermal resistances of cell components [9,14].

The heat generation rate, q, is given as

$$q = aJ\left[E_{oc} - E - T\frac{\mathrm{d}E_{oc}}{\mathrm{d}T}\right] + a_p r_p i_p^2 + a_n r_n i_n^2 \tag{13}$$

where a is the specific area of the battery (m^{-1}), J the current density (A m^{-2}) calculated by Eq. (8), E_{oc} the open-circuit potential of the cell (V), E the cell voltage (V), a_p and a_n the specific area of the positive and negative electrodes (m^{-1}), respectively, and i_p and i_n are the magnitudes of the vectors $\vec{i}_p$ and $\vec{i}_n$ obtained by Eqs. (3) and (4) (A m^{-1}), respectively. The first term of the right-hand side of Eq. (13) is the heat generated due to charge transfer at the electrode/electrolyte interfaces. This involves an irreversible part, representing the energy loss by the deviation of the cell potential from the open-circuit potential due to electrochemical polarization, and a reversible part, representing the heat proportional to $\mathrm{d}E_{oc}/\mathrm{d}T$ due to entropy change. The third and fourth terms arise from ohmic heating in the positive and negative electrodes, respectively [13,27,28]. The heat dissipation rate, q_{conv}, is derived as

$$q_{conv} = \frac{2h}{\mathrm{d}}(T - T_{air}) \tag{14}$$

where h is the convective heat transfer coefficient on the surfaces of the battery (W m^{-2} °C^{-1}), d the thickness of the battery in the direction perpendicular to the parallel electrodes (m), and T_{air} is the ambient temperature (°C). This term is rendered as in Eq. (14) by the approximation of a three-dimensional object into a two-dimensional one. Convective boundary condition applied on the boundaries of the electrode is written as

$$-k\frac{\partial T}{\partial n} = h_e(T - T_{air}) \tag{15}$$

where $\partial/\partial n$ denotes the gradient in the direction of the outward normal to the boundary and h_e is the effective convective heat transfer coefficient on the edge of the battery, which is modified to accommodate the effect of the aluminum pouch enveloping the edge of the electrodes.

3. Results and discussion

The solutions to the governing Eqs. (5), (6), and (12) subject to the associated boundary conditions were obtained by using the finite element method. Although numerical simulations were performed for the electrodes of many different shapes of a lithium-polymer battery, we will show the results for the electrodes of three different shapes because we think that three is enough to demonstrate the salient features of the modeling presented in this paper. The electrodes of three different shapes are referred to as the electrodes of types A–C. The schematic diagrams of the electrode shape for the types A–C are illustrated in Fig. 3(a–c), respectively. In order to test the validity of the modeling, the calculated discharge curves based on modeling for the 10 Ah battery fabricated by VK Corporation with the electrodes of type A shown in Figs. 1 and 3(a) are compared with the experimental data in Fig. 4. The experiments were per-

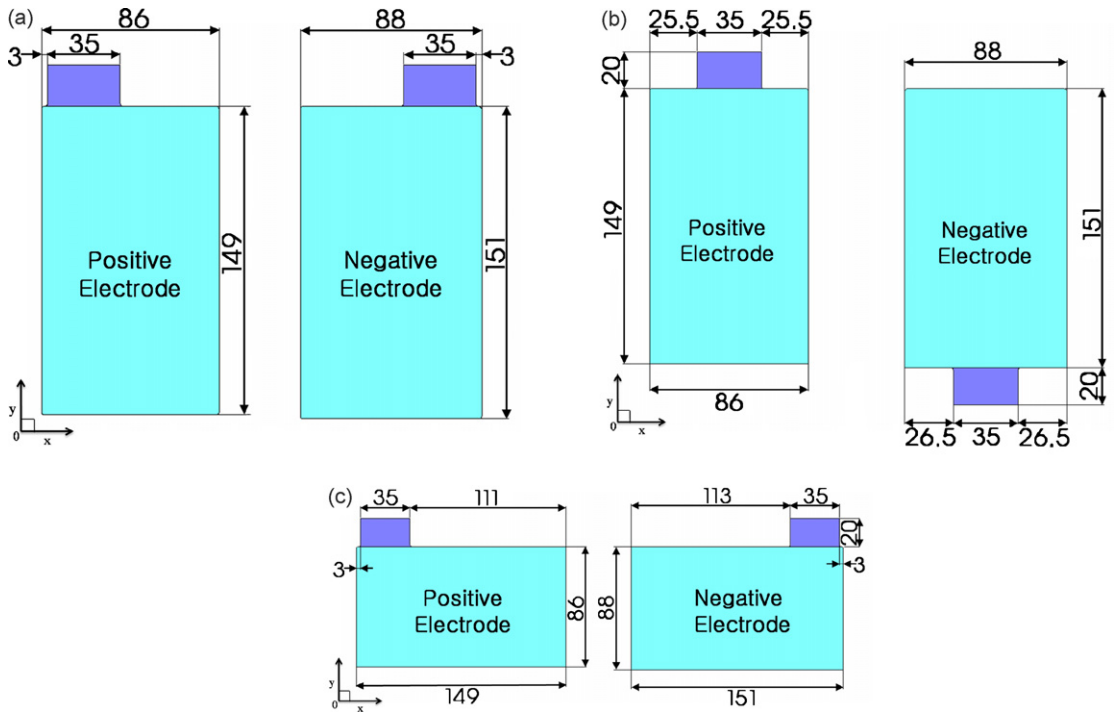

Fig. 3. Schematic diagrams of the electrode shapes for (a) type A, (b) type B, and (c) type C.

formed at room temperature. At various discharge rates from 1*C* to 5*C*, the experimental discharge curves are in good agreement with the modeling results based on the finite element method.

The distributions of the potential and current density on the electrodes during discharge are obtained as a function of time for various discharge rates. As an example, it is shown the distributions of the potential on the positive electrode, the potential on the negative electrode, and the current density for the battery with the electrodes of type A at the discharge time of 30 min with 1*C* rate in Fig. 5(a–c), respectively. In Fig. 5(a), the potential gradient on the positive electrode is seen to be most severe in the region where the tab is attached to the current collector. This is because all the current flows through the conducting current collector into the tab from the entire electrode plate. Again, the potential gradient on the negative electrode shown in Fig. 5(b) is the highest at the region near tab, because all the current has to flow from the tab through the entire electrode plate. Fig. 5(c) shows the non-uniform distributions of current density transferred from the negative electrode to the positive electrode of type A during the discharge with 1*C* rate.

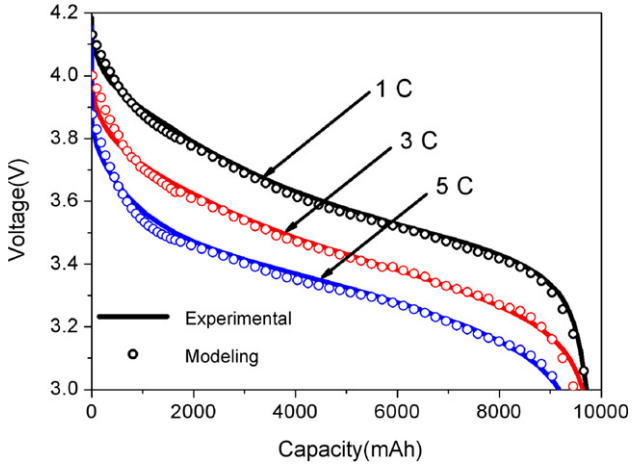

Fig. 4. Comparison between experimental and modeling discharge curves for the battery with the electrodes of type A at discharge rates of 1*C*, 3*C*, and 5*C*. Solid lines are experimental data and open circles are modeling results based on the finite element method.

After obtaining the distributions of the potential and current density on the electrodes during discharge, the temperature distributions of the battery can be calculated as a function of time for various discharge rates by using Eq. (12). As a demonstration, the temperature distributions based on the experimental IR image and the modeling after the discharge of 10.8 min with 5*C* rate are shown in Fig. 6. The overall appearances of the temperature distributions from the experiment and modeling are in good agreement. It is observed that the temperature near the current collecting tab of the positive electrode is higher than that of the negative electrode. This phenomenon is due to the fact that the electrical conductivity of the active material of the positive electrode is much lower than that of the negative electrode, although both of the current flows near the tabs of the positive and negative electrodes are similarly high. The maximum temperatures from the experiment and modeling are close to each other near the value of 58 °C, although the minimum temperature from the experiment is a bit higher than that from the modeling. The maximum and minimum temperatures from the experimental measurement for the battery with the electrodes of type A are compared with those predicted by the modeling in Fig. 7(a) and (b), respectively. The maximum temperatures from the experiment and modeling are in good agreement for the whole range of DOD at various discharge rates. However, the discrepancy

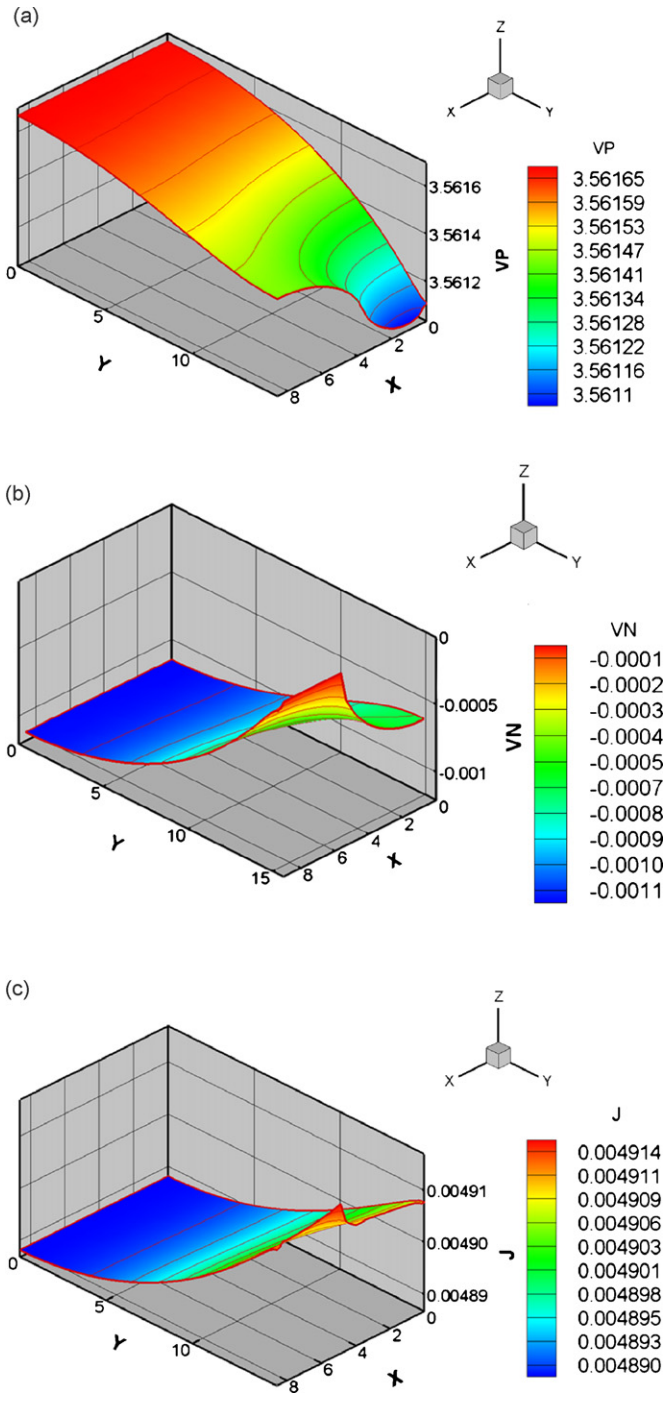

Fig. 5. Distributions of (a) the potential on the positive electrode, (b) the potential on the negative electrode, and (c) the current density on the electrodes of type A at the discharge time of 30 min with 1*C* rate.

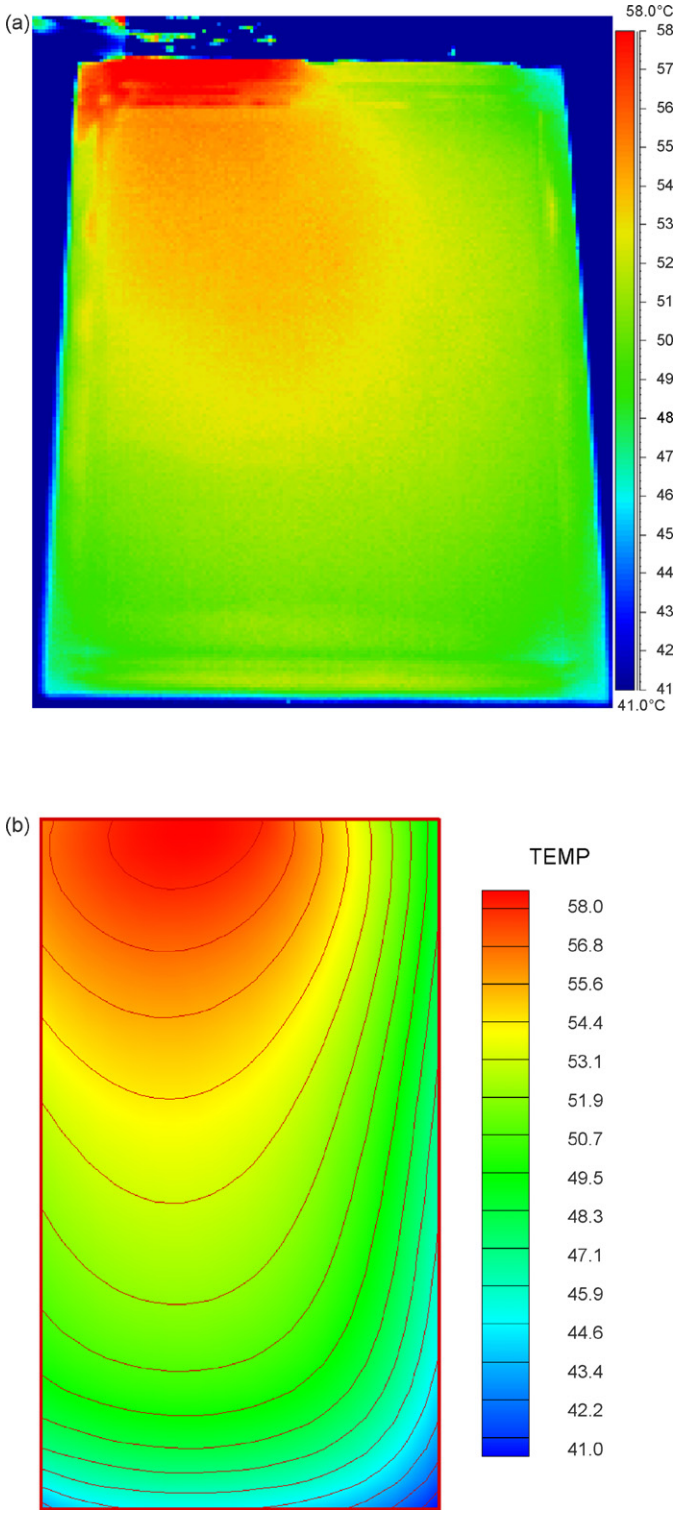

Fig. 6. Temperature distributions based on (a) the experimental IR image and (b) the modeling for the battery with the electrodes of type A at the discharge time of 10.8 min with 5*C* rate.

between the minimum temperatures from the experiment and modeling increases for the DOD values higher that 0.5 at the discharge rates of 3*C* and 5*C*.

To investigate the effect of placing of the current collecting tab on the thermal behavior of the battery, modeling is carried out for the battery with electrodes of type B. We used the same values of the parameters that we used to calculate the distributions of the potential and current density on the electrodes of type A during discharge in order to check whether the values of the parameters used for the electrodes of type A can be used for the electrodes of other types or not. The calculated discharge curves based on modeling for the electrodes of type B shown in Fig. 2(b) are compared with the experimental data in Fig. 8. At various discharge rates from 1*C* to

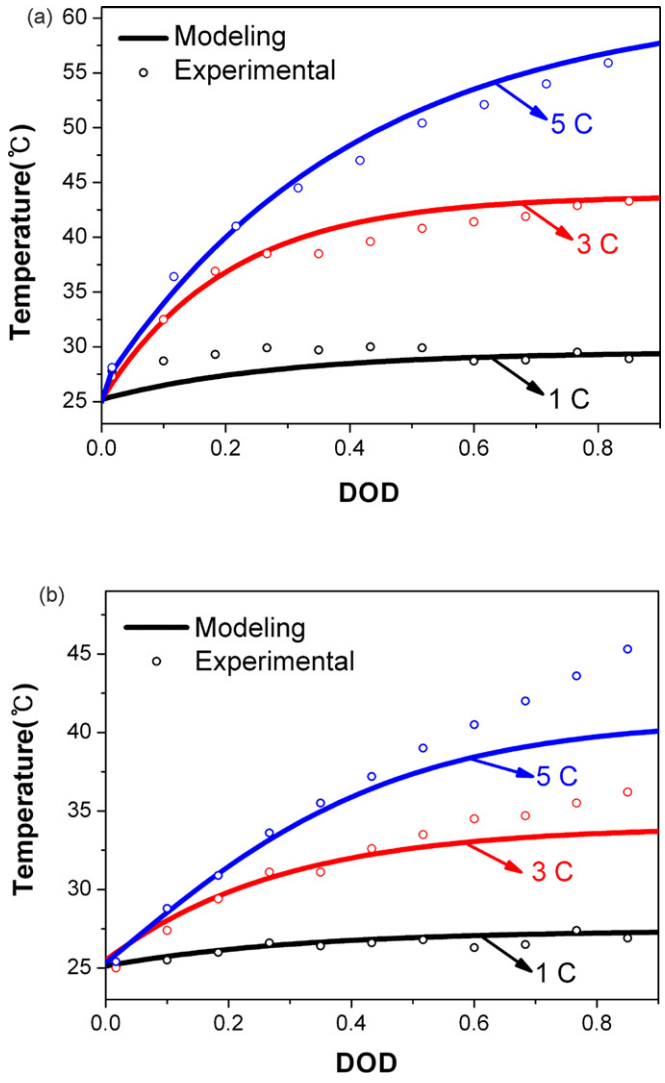

Fig. 7. Comparison between (a) the maximum temperatures and (b) the minimum temperatures from the experiment and modeling for the battery with the electrodes of type A at the discharge rates of 1*C*, 3*C*, and 5*C*.

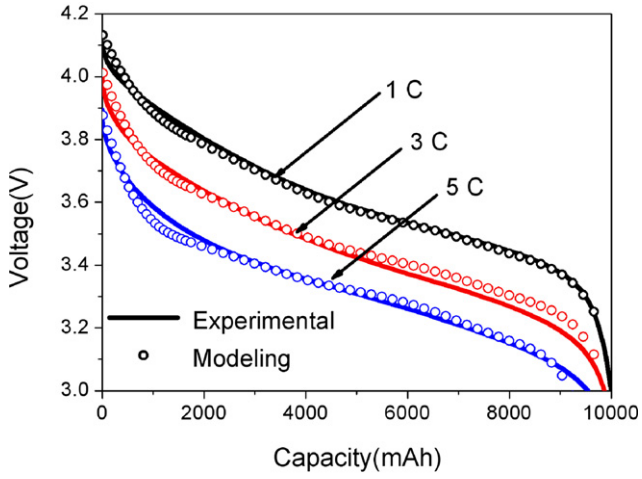

Fig. 8. Comparison between the experimental and modeling discharge curves for the battery with the electrodes of type B at the discharge rates of 1*C*, 3*C*, and 5*C*.

5*C*, the experimental discharge curves are in good agreement with the modeling results. We have confirmed that the discharge curves from the experiment agree well with those from the modeling for the electrodes of type C, for which the effect of aspect ratio of the electrodes on the thermal behavior was investigated. From these results, we have concluded that the parameters tuned for the electrodes of one geometry can be applied for the electrodes of other geometries as long as the materials and compositions of the electrodes and the manufacturing processes are the same.

In Fig. 9, the temperature distributions based on the experimental IR image and the modeling after the discharge of 10.8 min with 5*C* rate are shown for the battery with the electrodes of type B. The overall appearances of the temperature distributions from the experiment and modeling for the electrodes of type B are in good agreement. As in the case of the electrodes of type A, it is observed that the temperature near the current collecting tab of the positive electrode is higher than that of the negative electrode, because the electrical conductivity of the active material of the positive electrode is much lower than that of the negative electrode. The maximum temperatures from the experiment and modeling are close to each other near the value of 56 °C, and the minimum temperatures from the experiment and modeling are close to each other near the value of 43 °C. For the battery with the electrodes of type C, the temperature distributions based on the experimental IR image and the modeling after the discharge of 10.0 min with 5*C* rate are shown, in Fig. 10. The overall appearances of the temperature distributions from the experiment and modeling for the electrodes of type C are in good agreement. The maximum temperatures from the experiment and modeling are close to each other near the value of 54 °C, although the minimum temperature from the experiment is a bit higher than that from the modeling as for the case of the electrodes of type A. In Table 2, the maximum and minimum temperatures from the experimental measurement for the battery with the electrodes of types A–C are compared with those predicted by the modeling for the discharge rate of 5*C*, because the discrepancy between the temperatures from the experiment and modeling would be the highest as we have observed in Fig. 7. The maximum temperatures from the experiment and modeling are in good agreement for the whole range of DOD, but

Table 2
Maximum and minimum temperatures from the experiment and modeling for the discharge rate of 5*C*

Model	DOD [%]	Minimum temperature [°C]		Maximum temperature [°C]	
		Experimental	Modeling	Experimental	Modeling
Type A	30	34.4	33.5	44.5	44.5
	50	39.0	37.7	50.4	50.0
	90	47.0	40.0	57.8	58.7
Type B	30	32.9	35.3	43.7	41.9
	50	36.3	38.3	48.9	47.7
	90	42.8	43.7	57.0	55.6
Type C	30	35.7	33.6	43.0	43.1
	50	40.5	38.2	48.1	48.9
	83	45.4	38.9	53.7	55

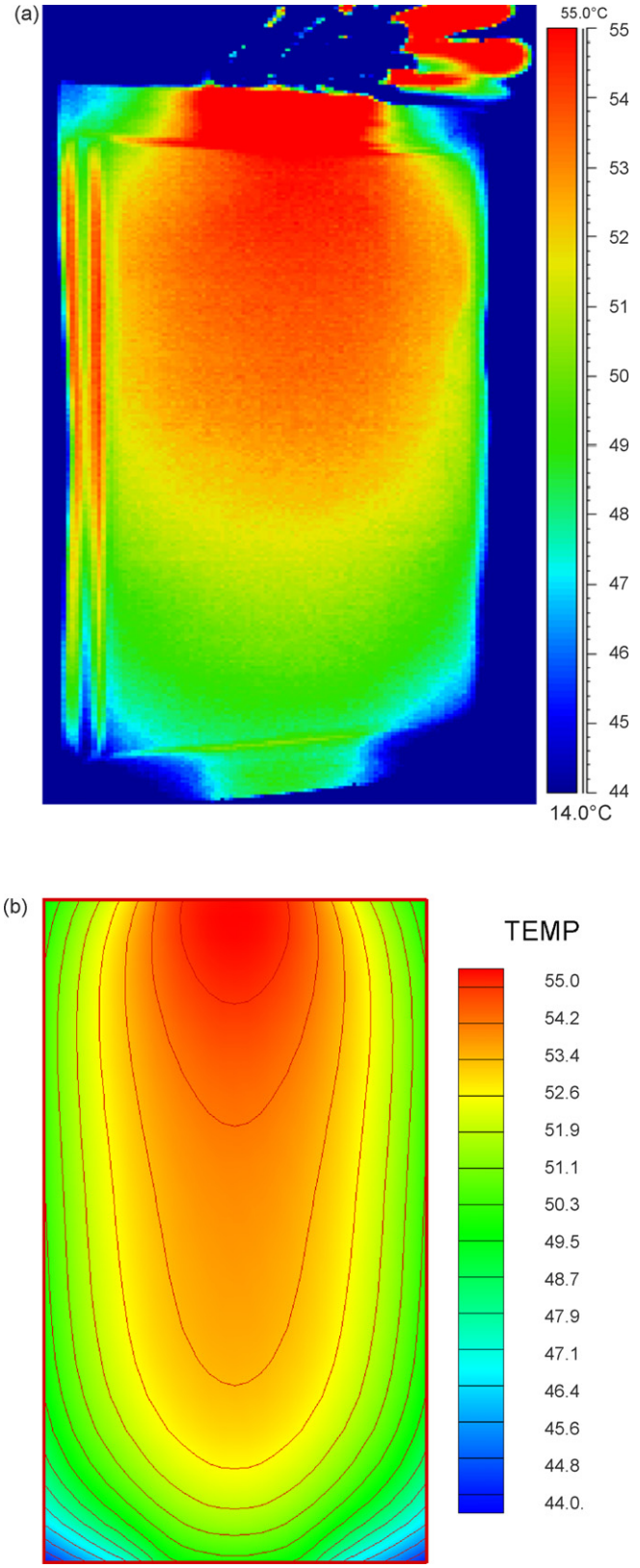

Fig. 9. Temperature distributions based on (a) the experimental IR image and (b) the modeling for the battery with the electrodes of type B at the discharge time of 10.8 min with 5*C* rate.

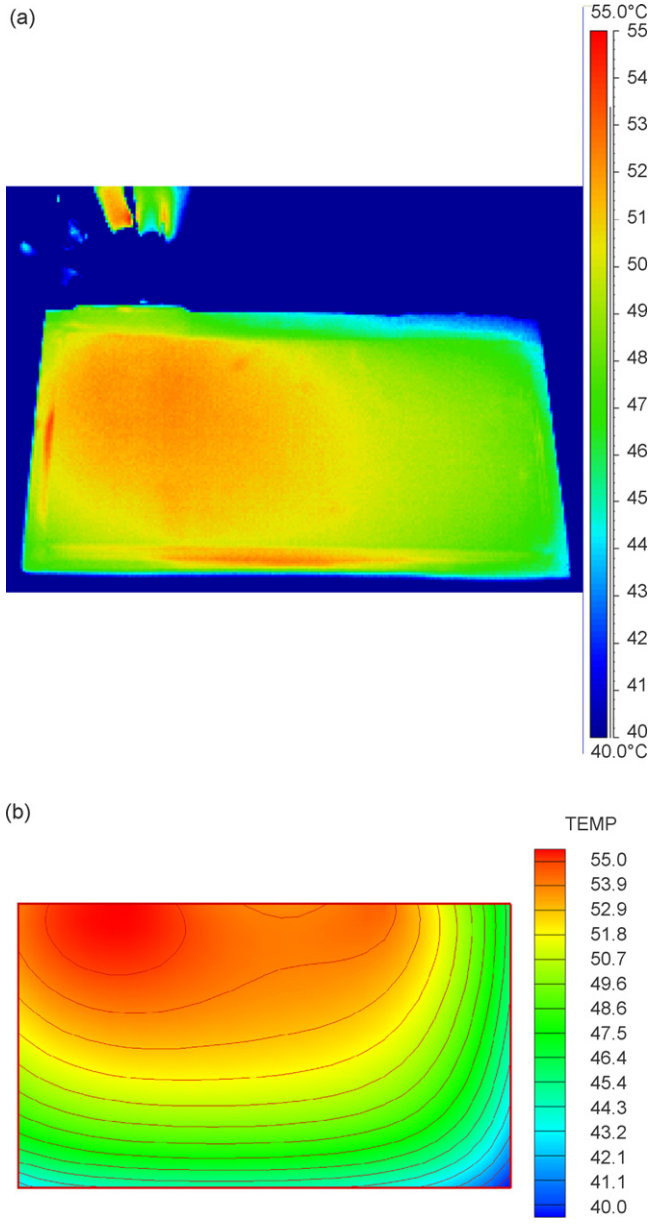

Fig. 10. Temperature distributions based on (a) the experimental IR image and (b) the modeling for the battery with the electrodes of type C at the discharge time of 10.0 min with 5*C* rate.

there are some discrepancies between the minimum temperatures from the experiment and modeling for the DOD values higher that 0.5 for the batteries with all different types of electrodes. If the electrodes of types A–C are evaluated in terms of the lower maximum temperature during discharge, the electrode of type B which has the current collecting tabs on the middle of opposite sides of the rectangular electrode is more preferable than those of types A and C which has the current collecting tabs at the ends of the same side of the rectangular electrode.

4. Conclusions

A mathematical procedure was developed to study the thermal behavior of a lithium-polymer battery. The two-dimensional

potential and current density distribution on the electrodes of a lithium-polymer battery were predicted as a function of discharge time by using the finite element method. Modeling was carried out for the electrodes of three different geometries to check the effect of the aspect ratio of the electrodes and the placing of current collecting tabs on the discharge behaviors of the battery. By comparing the experimental discharge curves with the modeling results at the discharge rates of 1C, 3C, and 5C, we confirmed that the parameters tuned for the electrodes of one geometry can be applied for the electrodes of other geometries as long as the materials and compositions of the electrodes and the manufacturing processes are the same. Then, based on the results of the modeling of potential and current density distributions, the heat generation rate as a function of discharge time and the position on the electrodes was calculated to predict the thermal behavior of the lithium-polymer battery. The two-dimensional temperature distributions from the experiment and modeling are in good agreement for the batteries with three different types of electrodes. The modeling methodology presented in this study, adopting a relatively simpler modeling approach as compared to the previously published papers by other researchers, may contribute to modifying the design of the electrode configuration.

Acknowledgements

This work was supported by the Ministry of Commerce, Industry, and Energy of Republic of Korea under the Generic Technology Development Program. One of the authors (C.B. Shin) acknowledges the Korea Science and Engineering Foundation (KOSEF R01-2006-000-10239-0) for providing partial financial supports for this work .

References

[1] G. Cedar, M. Doyle, P. Arora, Y. Fuentes, MRS Bull. 27 (2002) 619–623.
[2] J. Newman, K.E. Thomas, H. Hafezi, D.R. Wheeler, J. Power Sources 119–121 (2003) 838–843.
[3] Y. Chen, J.W. Evans, Electrochim. Acta 39 (1994) 517–526.
[4] C.R. Pals, J. Newman, J. Electrochem. Soc. 142 (1995) 3274–3281.
[5] C.R. Pals, J. Newman, J. Electrochem. Soc. 142 (1995) 3282–3288.
[6] S. Al-Hallaj, J.R. Selman, J. Power Sources 110 (2002) 341–348.
[7] K. Smith, C.-Y. Wang, J. Power Sources 160 (2006) 662–673.
[8] Y. Chen, J.W. Evans, J. Electrochem. Soc. 140 (1993) 1833–1838.
[9] Y. Chen, J.W. Evans, J. Electrochem. Soc. 141 (1994) 2947–2955.
[10] Y. Chen, J.W. Evans, J. Electrochem. Soc. 143 (1996) 2708–2712.
[11] L. Song, J.W. Evans, J. Electrochem. Soc. 145 (1998) 2327–2334.
[12] L. Song, J.W. Evans, J. Electrochem. Soc. 147 (2000) 2086–2095.
[13] P.M. Gomadam, J.W. Weidner, R.A. Dougal, R.E. White, J. Power Sources 110 (2002) 267–284.
[14] S.C. Chen, C.C. Wan, Y.Y. Wang, J. Power Sources 140 (2005) 111–124.
[15] K.H. Kwon, C.B. Shin, T.H. Kang, C.-S. Kim, J. Power Sources 163 (2006) 151–157.
[16] M.W. Verbrugge, J. Electrostatics 34 (1995) 61–85.
[17] D.R. Baker, M.W. Verbrugge, J. Electrochem. Soc. 146 (1999) 2413–2424.
[18] J. Newman, W. Tiedemann, J. Electrochem. Soc. 140 (1993) 1961–1968.
[19] G. Sikha, B.N. Popov, R.E. White, J. Electrochem. Soc. 151 (2004) A1104–A1114.
[20] G. Ning, B.N. Popov, J. Electrochem. Soc. 151 (2004) A1584–A1591.
[21] G. Ning, R.E. White, B.N. Popov, Electrochim. Acta 51 (2006) 2012–2022.
[22] D.W. Dees, V.S. Battaglia, A. Bélanger, J. Power Sources 110 (2002) 310–320.
[23] M. Doyle, J. Newman, A.S. Gozdz, C.N. Schmutz, J.-M. Tarascon, J. Electrochem. Soc. 143 (1996) 1890–1903.
[24] P. Arora, M. Doyle, A.S. Gozdz, R.E. White, J. Newman, J. Power Sources 88 (2000) 219–231.
[25] W. Tiedemann, J. Newman, in: S. Gross (Ed.), Battery Design and Optimization, The Electrochemical Society, Princeton, NJ, 1979, pp. 39–49.
[26] H. Gu, J. Electrochem. Soc. 130 (1983) 1459–1464.
[27] C.Y. Wang, V. Srinivasan, J. Power Sources 110 (2000) 364–376.
[28] V. Srinivasan, C.Y. Wang, J. Electrochem. Soc. 150 (2003) A98–A106.